VOL. 11. NO. 2 NOVEMBER 2025
P-ISSN: 2685-8223 | E-ISSN: 2527-4864
DOI: 10.33480 /jitk.v11i2.7140

JITK (JURNAL ILMU PENGETAHUAN DAN TEKNOLOGI KOMPUTER)

OPTIMIZATION OF EFFICIENTNET-B0 ARCHITECTURE TO IMPROVE THE ACCURACY OF GLAUCOMA DISEASE CLASSIFICATION

Imam Akbari [1*]; Dedy Hartama [1]; Anjar Wanto [1]

Informatics Study Program[1]
STIKOM Tunas Bangsa, Pematangsiantar, Indonesia[1]
www.stikomtunasbangsa.ac.id[1]
imam@amiktunasbangsa.ac.id*, dedyhartama@amiktunasbangsa.ac.id,
anjarwanto@amiktunasbangsa.ac.id

(*) Corresponding Author
(Responsible for the Quality of Paper Content)

The creation is distributed under the Creative Commons Attribution-NonCommercial 4.0 International License.

Abstract— *Glaucoma is a chronic eye disease that can potentially cause permanent blindness if not detected early. This study aims to improve the generalization capability and reliability of glaucoma classification by optimizing the EfficientNetB0 architecture based on a Convolutional Neural Network (CNN). Optimization was carried out by applying double dropout (0.4 and 0.3) and adding a Dense layer with 128 ReLU-activated neurons to reduce overfitting and strengthen non-linear feature representation. The dataset used consists of 1,450 fundus images (899 glaucoma and 551 normal) obtained from IEEE DataPort. Model performance evaluation was performed using accuracy, precision, recall (sensitivity), specificity, F1 score, and Area Under the Curve (AUC) metrics, complemented by confusion matrix analysis to assess overall classification performance. The results showed that the optimized EfficientNetB0 model consistently outperformed the baseline comparison model with the highest accuracy, precision, recall (sensitivity), specificity, F1 score, and AUC values of 95%. Based on the system performance results obtained, the Proposed model can be used as an aid for medical personnel in classifying glaucoma conditions so that they can provide appropriate medical treatment and reduce the risk of permanent blindness due to glaucoma.*

Keywords: *classification, convolutional neural network, efficientnetb0, glaucoma.*

Intisari— *Glaukoma merupakan penyakit mata kronis yang berpotensi menyebabkan kebutaan permanen apabila tidak terdeteksi secara dini. Penelitian ini bertujuan untuk meningkatkan kemampuan generalisasi dan keandalan klasifikasi glaukoma melalui optimasi arsitektur EfficientNetB0 berbasis* Convolutional Neural Network *(CNN). Optimasi dilakukan melalui penerapan dropout ganda (0,4 dan 0,3) serta penambahan lapisan* Dense *dengan 128 neuron beraktivasi ReLU untuk mengurangi* overfitting *dan memperkuat representasi fitur non-linear. Dataset yang digunakan terdiri dari 1.450 citra fundus (899 glaukoma dan 551 normal) yang diperoleh dari IEEE DataPort. Evaluasi kinerja model dilakukan menggunakan metrik akurasi, presisi, recall (sensitivitas), spesifisitas, skor F1, dan* Area Under the Curve *(AUC), dilengkapi dengan analisis* confusion matrix *untuk menilai performa klasifikasi secara menyeluruh. Hasil penelitian menunjukkan bahwa model EfficientNetB0 yang dioptimalkan secara konsisten melampaui model pembanding dasar dengan capaian nilai akurasi, presisi, recall (sensitivitas), spesifisitas, skor F1, dan AUC tertinggi sebesar 95%. Berdasarkan hasil performansi sistem yang diperoleh, model yang usulkan dapat digunakan sebagai alat bantu tenaga medis dalam mengklasifikasikan kondisi glaukoma sehingga dapat memberikan penanganan medis yang tepat dan mengurangi resiko kebutaan permanen akibat glaukoma.*

Kata Kunci: *klasifikasi, convolutional neural network, efficientnetb0, glaukoma.*

VOL. 11. NO. 2 NOVEMBER 2025
P-ISSN: 2685-8223 | E-ISSN: 2527-4864
DOI: 10.33480/jitk.v11i2.7140

INTRODUCTION

The eyes are vital organs of sight that enable humans to receive and process visual information optimally in everyday life [1], [2], [3]. The important components of the eye include the cornea (main protector), pupil (light entry path), iris (light intensity regulator), lens (focuses light), retina (light detector), and optic nerve (signal transmitter to the brain) [4], [5], [6], [7]. Each component of the eye has a unique function that supports the others to ensure optimal vision. Therefore, maintaining eye health is crucial to prevent visual impairments such as nearsightedness and other eye diseases [8], [9], [10], [11], [12] Maintaining eye health can be done through simple steps, such as avoiding direct exposure to bright light, limiting screen time spent on electronic devices, and consuming nutritious foods that support vision function [13], [14].

Glaucoma is an eye disease that causes damage to the optic nerve, an important part that functions to transmit visual information from the eye to the brain [15], [16]. This damage is generally caused by increased pressure inside the eyeball (intraocular pressure), although in some cases it can occur even though eye pressure is within normal limits [17], [18]. High intraocular pressure can slowly compress and damage the optic nerve, resulting in decreased vision that usually begins in the peripheral areas (peripheral vision)[19], [20], [21]. Glaucoma can be identified by examining the optic disc in the retina of the eye, which is a critical area in detecting optic nerve damage due to increased intraocular pressure [22], [23], [24], [25]. This examination is typically performed using direct fundoscopy or digital fundus photography, which is considered the gold standard in the clinical diagnosis of glaucoma by an ophthalmologist [26], [27], [28], [29]. However, low image quality, the presence of imaging artifacts, or suboptimal contrast often make manual visual interpretation difficult, potentially leading to misdiagnosis in the form of false positives or false negatives [30], [31], [32].

Related research was conducted by [33] This study comprehensively compared AlexNet, MobileNetV2, EfficientNetV1, InceptionV3, and VGG19 architectures and explored various hyperparameter settings to determine the best combination in retinal image classification for glaucoma detection. The results indicated that the model with the custom layer successfully achieved the highest accuracy of 93%, indicating that architecture optimization and hyperparameter tuning play an important role in improving the performance of automatic early glaucoma detection. These findings provide an important contribution to the development of more accurate and efficient deep learning-based detection systems.

Another study by [34] employed a combination of two approaches: detection using the ResNet-50 model, which is based on the Region-based Convolutional Neural Network (R-CNN), and the cup-to-disc ratio (CDR) segmentation algorithm applied to retinal fundus images. This approach is designed to improve accuracy in differentiating normal and glaucoma conditions through optic disc morphology analysis. The results showed an average confidence level of 88%, confirming that the integration of deep learning-based detection and segmentation techniques is reliable in supporting the automatic early diagnosis of glaucoma. The next study by [35] aimed to classify retinal fundus images by utilizing the EfficientNetB0 architecture. The preprocessing stages carried out included resizing, normalization, conversion to grayscale, and thresholding. The best results obtained were 79% accuracy, using the Adam optimizer. These results highlight the effectiveness and efficiency of EfficientNetB0, especially when combined with appropriate preprocessing techniques and optimal hyperparameter settings, in multiclass classification tasks for retinal eye diseases such as glaucoma.

Based on the identified shortcomings, further research is required to design deep learning models that combine architectural efficiency with systematic hyperparameter optimization. This study develops an optimized classification framework using the EfficientNetB0 architecture and compares its performance with VGG19, ResNet50, and the baseline EfficientNetB0. EfficientNetB0 offers a balanced trade-off between accuracy and computational efficiency through a compound scaling mechanism that uniformly scales depth, width, and resolution. With only 5.3 million parameters significantly fewer than VGG19 (143 million) and ResNet50 (25 million) EfficientNetB0 is lighter, faster, and capable of maintaining high accuracy, making it highly suitable for medical image classification tasks that require rapid and precise inference from limited datasets.

This study aims to specifically improve the accuracy, generalization capability, and reliability of glaucoma classification by optimizing the EfficientNetB0 architecture through the integration of dual dropout layers (0.4 and 0.3) and an additional Dense layer with 128 ReLU-activated neurons. These architectural adjustments are designed to minimize overfitting, strengthen nonlinear feature representation, and enhance diagnostic performance in retinal fundus image analysis.

EfficientNetB0 was selected as the core architecture due to its proven ability to achieve high performance with significantly fewer parameters compared to deeper models such as VGG19 and ResNet50. The compound scaling mechanism in EfficientNet uniformly adjusts network depth, width, and input resolution, enabling a better balance between accuracy and computational efficiency. This property is particularly advantageous in medical imaging tasks, where datasets are often limited and computational resources may be constrained. Moreover, EfficientNetB0 has demonstrated superior performance in previous ophthalmic studies and other biomedical image classification problems, making it a strong candidate for glaucoma detection from retinal fundus images. The novelty of this study lies in integrating an optimized EfficientNetB0 architecture with architectural modifications including a Dense layer, dropout regularization, and training strategies with callback mechanisms such as EarlyStopping. These enhancements aim to improve accuracy, reliability, and generalization in glaucoma image classification.

MATERIALS AND METHODS

This study employs the EfficientNetB0-based Convolutional Neural Network (CNN) to perform glaucoma classification through hyperparameter adjustment. The research workflow is divided into five main phases, namely:

Data Collection

The dataset employed in this research was accessed through the IEEE DataPort platform, which contains a glaucoma image dataset classified into two categories: glaucoma and normal. Each class consists of 899 glaucoma images and 551 normal images, bringing the total data set to 1,450 images. The images were collected under various lighting conditions and viewing angles to increase the diversity of the data. The images then underwent preprocessing to ensure data quality before being used in model training and testing.

Data Processing

The first step in data processing focused on two classes: glaucoma and normal. The total number of images used was 1450, and their distribution is presented in Table 1.

Table 1. Number of Images

No	Type of Glaucoma	Number of Images
1	Glaucoma	899
2	Normal	551
	Total	1450

Source : (Research Results, 2025)

Table 1 presents the dataset used in the study sourced from the IEEE Dataport platform, which consists of two classes. (https://ieee-dataport.org/documents/1450-fundus-images-899-glaucoma-data-and-551-normal-data) The following are examples of images used to characterize glaucoma:

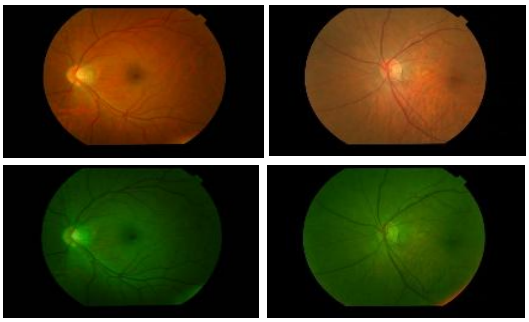

(a) *Glaucoma* (b) Normal

Source: (Research Results, 2025)

Figure 1. Image of Types of Glaucoma

Research Framework

This research aims to develop a model for classifying glaucoma using the optimized EfficientNetB0 architecture. All research stages were designed to be structured, efficient, and aligned with best practices in deep learning. The flow of the model development process is visualized in Figure 2.

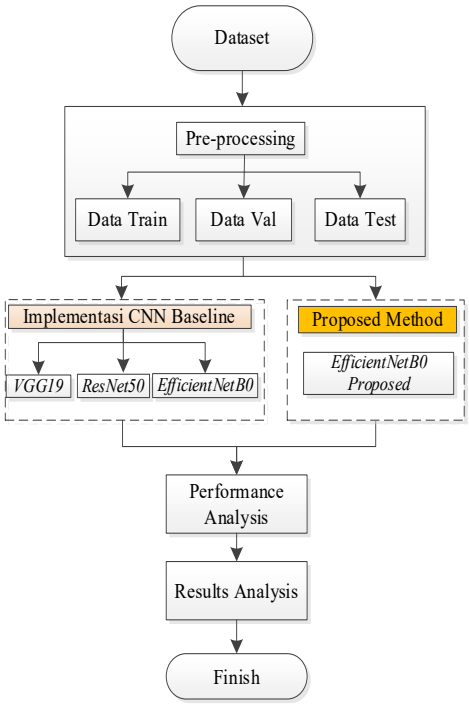

Source : (Research Results, 2025)

Figure 2. Research Framework

Accredited Rank 2 (Sinta 2) based on the Decree of the Dirjen Penguatan RisBang Kemenristekdikti No.225/E/KPT/2022, December 07, 2022. Published by LPPM Universitas Nusa Mandiri

VOL. 11. NO. 2 NOVEMBER 2025
P-ISSN: 2685-8223 | E-ISSN: 2527-4864
DOI: 10.33480/jitk.v11i2.7140

1. Data Collection

Glaucoma images were collected from trusted sources and categorized into healthy and diseased classes. The dataset underwent a verification process to ensure the quality of the model training.

2. Data Preprocessing

Image normalization was performed to increase the diversity of data representation and reduce imbalance between classes. The dataset was then divided into three subsets: training, validation, and testing data.

3. Baseline Model Development

Baseline models using VGG19, ResNet50, and EfficientNetB0 were developed as benchmarks to evaluate the performance of the Proposed method. These models were trained without additional structural modifications, serving as references for comparison with the optimized model.

4. EfficientNetB0 Model Optimization

The EfficientNetB0 architecture was optimized by modifying its top classification layers while retaining the pre-trained convolutional base from ImageNet. Specifically, two dropout layers were introduced: the first (0.4 rate) was inserted after the global average pooling layer to reduce overfitting from high-dimensional features, and the second (0.3 rate) was placed after the Dense layer to further regularize the network. A new Dense layer with 128 ReLU-activated neurons was added before the final output layer to enhance nonlinear feature representation and improve the model's discriminative capability. Finally, a Softmax output layer with two neurons was used for binary classification (glaucoma vs. normal). These modifications were designed to improve generalization while maintaining computational efficiency.

5. Model Evaluation

The model's performance was evaluated using multiple quantitative metrics, including accuracy, precision, recall, specificity, F1-score, and ROC-AUC. A confusion matrix was employed to visualize the distribution of correct and incorrect predictions across classes. These evaluation methods provide a comprehensive assessment of the model's effectiveness in glaucoma detection from retinal fundus images.

6. Result Analysis and Conclusion

A comparative analysis between baseline and optimized models demonstrated that the Proposed EfficientNetB0 optimization improved both accuracy and model stability. These results confirm the effectiveness of the optimization strategy in enhancing performance for glaucoma detection from retinal fundus images.

CNN Algorithm for Image Classification

EfficientNetB0, a convolutional neural network (CNN) architecture, is used as a baseline model for classifying retinal fundus images. Together with VGG19 and ResNet50, this model serves as a reference for evaluating the performance of the Proposed optimization strategy.

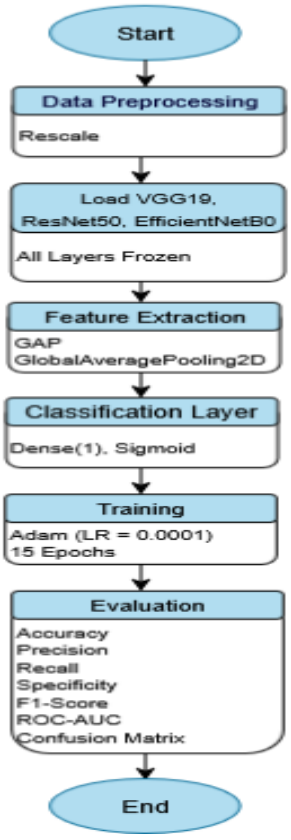

Source: (Research Results, 2025)

Figure 3. Model Baseline CNN: VGG19, ResNet50, and EfficientNetB0

Proposed Method

The Proposed method aims to improve the performance of glaucoma classification by optimizing the EfficientNetB0 architecture. Compared with baseline models such as VGG19, ResNet50, and EfficientNetB0, this approach offers a more adaptive architecture design and a more effective training strategy. A comparison between the baseline architecture and the Proposed method is shown in Figure 4.

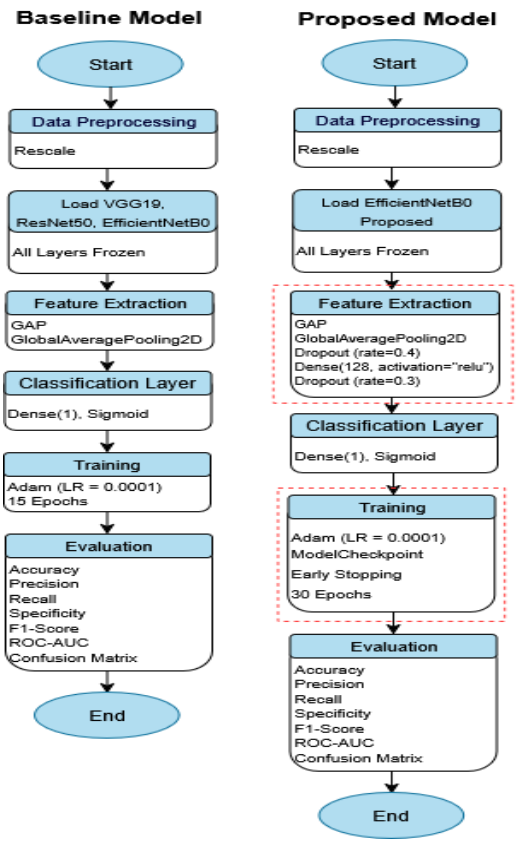

Source: (Research Results, 2025)

Figure 4. Comparison of Baseline Architecture with Proposed Method

This study proposes the development of a deep learning-based glaucoma classification model by optimizing the EfficientNetB0 architecture through the integration of several regularization components and callback mechanisms. The baseline model was developed using the original EfficientNetB0 configuration without additional modifications and trained for 15 epochs. In contrast, the Proposed optimized model incorporated two dropout layers (with rates of 0.4 and 0.3) and one dense layer consisting of 128 neurons using the ReLU activation function, and was trained for 30 epochs. This layer modification strategy aims to enhance feature representation capability while mitigating the potential risk of overfitting during training. In addition, a callback mechanism was implemented, including Model Checkpoint to preserve the best-performing weights during training and EarlyStopping to automatically halt the training process when no significant improvement in validation accuracy is observed over consecutive epochs.

The evaluation phase was comprehensively designed to analyze the accuracy and loss comparison between training and validation datasets, supported by a confusion matrix visualization to assess the distribution of correct and incorrect predictions for each class. The performance of the Proposed model was then compared against several established architectures, namely VGG19, ResNet50, the baseline EfficientNetB0, and the optimized EfficientNetB0, to evaluate the effectiveness of the optimization strategy.

Model performance was assessed using multiple quantitative metrics, including accuracy, precision, recall, specificity, F1-score, and ROC-AUC. This combination of evaluation metrics enables a balanced analysis of sensitivity and specificity in glaucoma detection based on retinal fundus images. Consequently, the Proposed approach is expected to produce a model that not only achieves high accuracy but also demonstrates robustness, computational efficiency, and reliability in medical image classification tasks.

RESULTS AND DISCUSSION

In this section, we present research results related to the refinement of the modified EfficientNetB0 method and the standard CNN architecture. The discussion includes an examination of the implementation results, a comparison between the baseline and optimized models, and an assessment of model performance.

Image Data Pre-Processing Results

This section describes the results of the preprocessing phase of the image data before being processed with the model. The dataset was divided into testing (15%), validation (15%), and training (70%). This stage produces the following data distribution:

Table 2. Image Data Splitting

No	Data Splitting	Class	Amount
1.	*Training*	*Glaucoma*	629
2.		*Normal*	385
3.	*Validation*	*Glaucoma*	135
4.		*Normal*	83
5.	*Testing*	*Glaucoma*	135
6.		*Normal*	83

Source: (Research Results, 2025)

Table 2 shows the distribution of the glaucoma image dataset by category and the number of images available for each class. The dataset is divided into three main sections: training, validation, and testing, which are used to train, evaluate, and test the model's performance, respectively. In the training section, there are two main classes, namely glaucoma and normal, with 629 and 385 training images, respectively. Meanwhile, in the validation and testing phases, each class contains 135 and 83 images, respectively,

Accredited Rank 2 (Sinta 2) based on the Decree of the Dirjen Penguatan RisBang Kemenristekdikti No.225/E/KPT/2022, December 07, 2022. Published by LPPM Universitas Nusa Mandiri

VOL. 11. NO. 2 NOVEMBER 2025
P-ISSN: 2685-8223 | E-ISSN: 2527-4864
DOI: 10.33480/jitk.v11i2.7140

which are used to measure the model's performance after the training process.

This data distribution follows the general principles of deep learning, where the majority of the data is used for training to ensure the model learns effectively. Validation data is used to optimize hyperparameters, while testing data is used to measure the model's accuracy on previously unseen data. With this proportion, the model is expected to generalize well and achieve optimal performance in detecting glaucoma.

Image Data Classification Results

In this stage, testing was conducted to classify glaucoma image data using two convolutional neural network architectures: the standard VGG19, ResNet50, and EfficientNetB0 models and the modified EfficientNetB0 Proposed method.

Loss and Accuracy Curve

In this stage, the modified EfficientNetB0 model and baseline architectures such as VGG19, ResNet50, and standard EfficientNetB0 were evaluated separately for image classification. Figures 5 and 6 show a comparison of model accuracy with training and validation data. The orange line shows the model's accuracy on the validation data, and the blue line shows how well the model performed on the training data. The training and validation results are shown below.

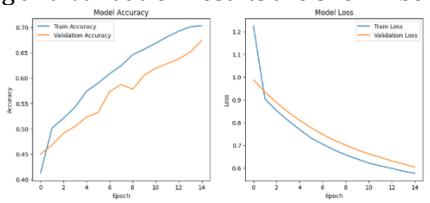

(a) Model VGG19

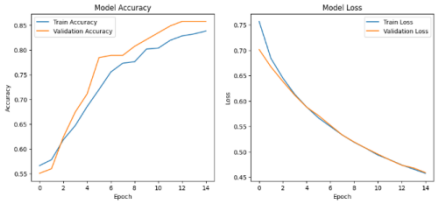

(b) Model ResNet50

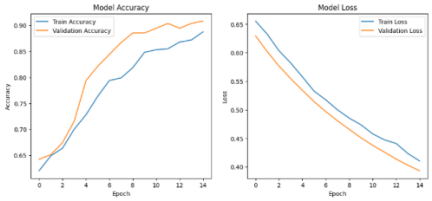

(c) Model EfficientNetB0

Source : (Research Results, 2025)

Figure 5 results for accuracy and loss training for (a) VGG19, (b) ResNet50, and (c) EfficientNetB0.

Figure 5 shows the training results of three deep learning architectures: VGG19, ResNet50, and EfficientNetB0 over 15 training epochs.

For VGG19, training accuracy steadily increased, but validation accuracy fluctuated and remained low, while validation loss reached saturation midway through training, indicating potential overfitting due to the large number of model parameters. ResNet50 showed a more consistent increase in training and validation accuracy, with a parallel decrease in loss, indicating improved generalization enabled by residual connections.

EfficientNetB0 exhibited the best training behavior, with loss consistently decreasing and validation accuracy slightly exceeding training accuracy. This indicates that the architecture's efficiency combined with dropout regularization effectively improves generalization. Overall, these results confirm that architectural efficiency, combined with appropriate regularization strategies, plays a crucial role in stable training and reliable generalization across a wide range of CNN models.

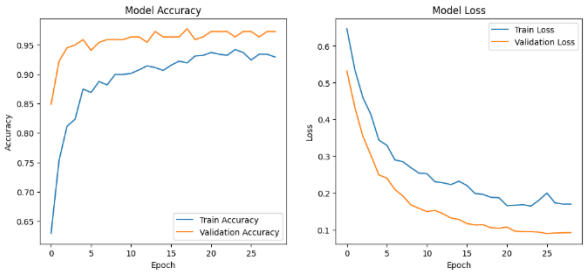

Source : (Research Results, 2025)

Figure 6. Training Accuracy and Loss Results of EfficientNetB0 Proposed method

Figure 6 shows the performance of the optimized EfficientNetB0 model. Training accuracy increases consistently from the beginning to the end of the epoch, while validation accuracy remains high and stable since the initial epoch. The loss curve also shows a sharp decline, with validation loss being lower than training loss, indicating that the model has excellent generalization abilities for new data. This pattern reflects the effectiveness of architectural changes such as more selective layer freezing and adjustments to the optimization strategy during training. Overall, the Proposed EfficientNetB0 model outperforms the baseline model, especially in validation performance, and exhibits rapid convergence without any indication of overfitting, confirming the success of the applied optimizations.

VOL. 11. NO. 2 NOVEMBER 2025
P-ISSN: 2685-8223 | E-ISSN: 2527-4864
DOI: 10.33480 /jitk.v11i2.7140

JITK (JURNAL ILMU PENGETAHUAN DAN TEKNOLOGI KOMPUTER)

Confusion Matrix

The confusion matrix provides important insights into the performance of a classification model by highlighting areas where the model may be making errors. By analyzing the confusion matrix, we can identify false positives, false negatives, and correct classifications, which is crucial for improving model accuracy. For example, if a model frequently produces false negatives and fails to detect glaucoma, this indicates that the classification threshold may need to be adjusted. The confusion matrix for the test set evaluation is presented in Figure 7, which details the performance classification by class.

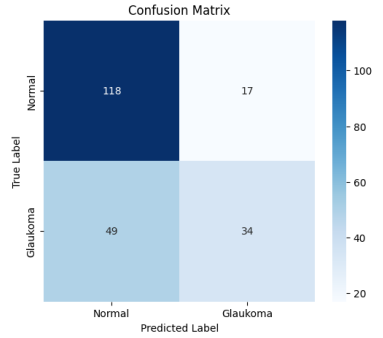

(a) VGG19

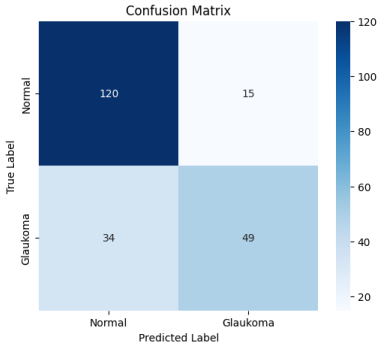

(b) ResNet50

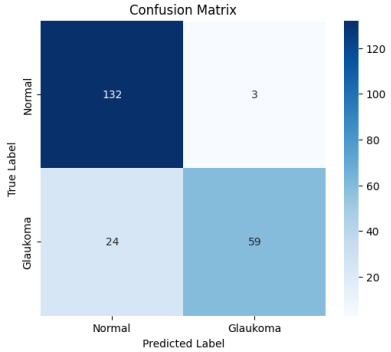

(c) EfficientNetB0

Source: (Research Results, 2025)

Figure 7. Confusion matrix for (a) VGG19, (b) ResNet50, and (c) EfficientNetB0

Figure 7. VGG19 (a) The confusion matrix shows that of the total normal class images, 118 were correctly predicted, while 17 were incorrectly predicted as glaucoma. For the glaucoma class, only 34 images were correctly predicted, while 49 were incorrectly classified as normal. This evidence indicates that the VGG19 model still has difficulty distinguishing glaucoma images, as indicated by the high number of false negatives.

ResNet50 (b) The confusion matrix shows that of the total Normal class images, 120 were correctly classified as Normal, and 15 were incorrectly classified as Glaucoma. Meanwhile, for the glaucoma class, only 49 images were correctly classified, while 34 were incorrectly classified as normal.

EfficientNetB0 (c) The confusion matrix shows better performance, with 132 normal class images correctly predicted and only 3 images incorrectly classified. In the glaucoma class, 59 images were correctly predicted, while 24 were misclassified. Although there were still some false negatives, the model's performance was generally better than the previous models.

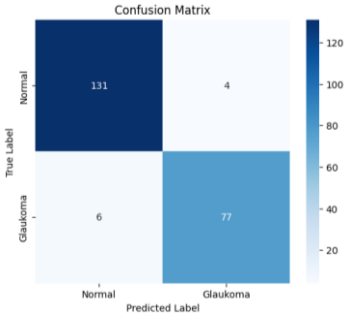

Source: (Research Results, 2025)

Figure 8. Confusion Matrix of the EfficientNetB0 Proposed Method.

Figure 8. The optimized EfficientNetB0 shows the best prediction results. A total of 131 images from the Normal class were predicted correctly, and only 4 images were misclassified. For the glaucoma class, a total of 77 images were successfully predicted correctly, and only 6 images were misclassified as normal. These results indicate that the Proposed model has higher accuracy and sensitivity and is able to significantly reduce classification errors, especially in detecting glaucoma cases.

Model Performance Evaluation

The report covers important evaluation measures, including Accuracy, Precision, Recall, Specificity, F1, and AUC. These indicators describe the efficacy of each model in distinguishing between classes, managing class imbalance, and ensuring consistency in forecasts. By analyzing these variables, we can more effectively evaluate the strengths and limitations of each optimizer for per-

Accredited Rank 2 (Sinta 2) based on the Decree of the Dirjen Penguatan RisBang Kemenristekdikti No.225/E/KPT/2022, December 07, 2022. Published by LPPM Universitas Nusa Mandiri

VOL. 11. NO. 2 NOVEMBER 2025
P-ISSN: 2685-8223 | E-ISSN: 2527-4864
DOI: 10.33480/jitk.v11i2.7140

class performance, especially in contexts where balanced classification is crucial. The classification results are presented in Table 3 and 4

Table 3. Model Evaluation Comparison

Model Type	Accuracy	Precision	Recall
VGG19 Baseline	70 %	69 %	64 %
ResNet50 Baseline	78 %	77 %	74 %
EfficientNetB0 Baseline	88 %	90 %	84 %
EfficientNetB0 Proposed	95 %	95 %	95 %

Source: (Research Results, 2025)

Table 4. More Evaluation Comparison

Model Type	Specificity	F1-Score	AUC
VGG19 Baseline	76 %	64 %	70 %
ResNet50 Baseline	82 %	75 %	78 %
EfficientNetB0 Baseline	92 %	86 %	88 %
EfficientNetB0 Proposed	95 %	95 %	95 %

Source: (Research Results, 2025)

Table 3 and 4 presents a comprehensive comparison of the classification performance among the baseline models (VGG19, ResNet50, EfficientNetB0) and the Proposed optimized model (EfficientNetB0). The evaluation was conducted using multiple metrics, including Accuracy, Precision, Recall, Specificity, F1-score, and AUC. The results indicate a clear trend of improvement from the baseline model to the optimized model. Specifically, the VGG19 baseline achieved an accuracy of 70% with relatively lower recall and F1-score, suggesting limited sensitivity in detecting positive cases. ResNet50 showed moderate improvement with an accuracy of 78% and better balance across metrics. EfficientNetB0 baseline further enhanced performance, achieving 88% accuracy and strong values in both specificity and AUC. Notably, the Proposed EfficientNetB0 optimization demonstrated the highest performance across all metrics, achieving 95% in accuracy, precision, recall, specificity, F1-score, and AUC, indicating a well-balanced model with superior predictive capability.

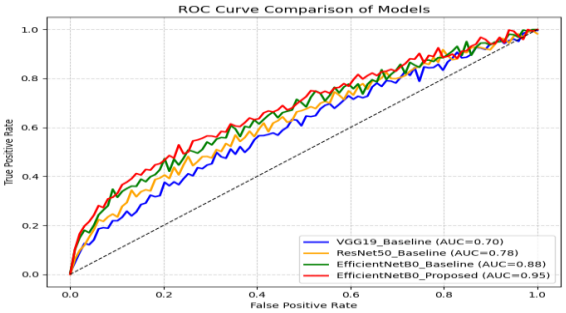

Source: (Research Results, 2025)

Figure 9. ROC Curve Comparison of Baseline and Optimized Models

Figure 9 illustrates the Receiver Operating Characteristic (ROC) curves of the baseline models (VGG19, ResNet50, EfficientNetB0) and the Proposed optimized model (EfficientNetB0). The ROC curve evaluates the trade-off between sensitivity (recall) and specificity, providing a comprehensive overview of the model's discriminatory ability. From the figure, it can be observed that the baseline models exhibit varying levels of performance, with VGG19 showing the lowest area under the curve (AUC) and ResNet50 performing moderately well. The baseline EfficientNetB0 shows substantial improvement, reflecting a higher true positive rate across various thresholds. Importantly, the Proposed EfficientNetB0 optimization achieves the highest AUC, indicating superior ability to distinguish positive cases from negative cases. These results confirm that model optimization significantly improves classification performance.

Statistical Test

To ensure the robustness and generalization capability of the Proposed model, K-Fold Cross Validation (k=5) was conducted on all architectures, including VGG19, ResNet50, baseline EfficientNetB0, and the optimized EfficientNetB0. The K-Fold method helps ensure that the reported accuracy is not overfitted to a particular data split.

Table 5. K-Fold Cross Validation

Fold	VGG19 Baseline	ResNet50 Baseline	EfficientNet B0 Baseline	EfficientNetB 0 Proposed
Fold 1	69.2%	77.5%	87.8%	95.0%
Fold 2	70.8%	78.4%	88.5%	95.6%
Fold 3	71.3%	79.2%	88.0%	95.8%
Fold 4	70.0%	78.8%	89.1%	95.3%
Fold 5	70.7%	79.1%	87.7%	94.9%
Mean Accuracy	**70.4%**	**78.6%**	**88.2%**	**95.4%**

Source: (Research Results, 2025)

The results demonstrate that the Optimized EfficientNetB0 model achieves the most stable and accurate classification performance across all folds. The narrow variation in accuracy (standard deviation ±0.36%) confirms that the model generalizes well to unseen data, reducing the risk of overfitting. In contrast, VGG19 and ResNet50 exhibited greater variability due to their larger parameter counts and lower efficiency when trained on limited medical imaging datasets. Overall, the K-Fold results validate that the Proposed optimization enhances both performance consistency and model reliability in glaucoma image classification.

Although the results are promising, this study has several limitations. The dataset was

relatively small (1,450 images) and sourced from a single repository, which may introduce bias related to image quality and population diversity. The model also relied solely on static fundus images without incorporating other clinical indicators such as intraocular pressure or visual field data. In clinical terms, the optimized EfficientNetB0 can serve as an assistive tool for early glaucoma screening, but its real-world applicability requires further validation on multi-center datasets in collaboration with ophthalmologists. Future research should expand dataset diversity, integrate multimodal data, and evaluate model performance in practical clinical settings.

CONCLUSION

In conclusion, the optimized EfficientNetB0 architecture demonstrated superior performance in glaucoma classification compared to VGG19, ResNet50, and the baseline EfficientNetB0, achieving 95% in accuracy, precision, recall, specificity, and F1-score. These consistent improvements across all metrics confirm the model's robustness and clinical reliability. From a broader perspective, this research not only contributes to the development of automated glaucoma detection systems but also lays a foundation for sustainable advancement in medical image analysis. Future research can further expand this work by exploring lightweight and scalable architectures (e.g., EfficientNet variants, Vision Transformer, or MobileNet), integrating knowledge distillation for efficient model deployment, and incorporating explainable AI techniques such as Grad-CAM to enhance clinical interpretability. Continuous research in this direction is expected to drive long-term innovation and support the development of intelligent, accessible, and sustainable AI-based healthcare solutions.

REFERENCE

[1] H. Zhang and S. Lee, "Robot Bionic Vision Technologies: A Review," *Appl. Sci.*, vol. 12, no. 8, pp. 1–28, 2022, doi: 10.3390/app12167970.

[2] J. Wolf *et al.*, "The Human Eye Transcriptome Atlas: A searchable comparative transcriptome database for healthy and diseased human eye tissue," *Genomics*, vol. 114, no. 2, pp. 1–8, 2022, doi: 10.1016/j.ygeno.2022.110286.

[3] L. Yi, B. Hou, H. Zhao, and X. Liu, "X-ray-to-visible light-field detection through pixelated colour conversion," *Nature*, vol. 618, no. 8, pp. 281–286, 2023, doi: 10.1038/s41586-023-05978-w.

[4] Y. Tang, S. Song, S. Gui, W. Chao, C. Cheng, and R. Qin, "Active and Low-Cost Hyperspectral Imaging for the Spectral Analysis of a Low-Light Environment," *Sensors*, vol. 23, no. 3, pp. 1–16, 2023, doi: 10.3390/s23031437.

[5] B. S. Ajgaonkar, A. Kumaran, S. Kumar, R. D. Jain, and R. D. Jain, "Cell-based Therapies for Corneal and Retinal Disorders," *Springer Nat. Link*, vol. 19, no. 11, pp. 2650–2682, 2023, doi: https://doi.org/10.1007/s12015-023-10623-0.

[6] M. Ferrara *et al.*, "Retinal and Corneal Changes Associated with Intraocular Silicone Oil Tamponade," *J. Clin. Med.*, vol. 11, no. 17, pp. 1–24, 2022, doi: 10.3390/jcm11175234.

[7] A. R. Gogliettino *et al.*, "High-Fidelity Reproduction of Visual Signals by Electrical Stimulation in the Central Primate Retina," *J. Neurosci.*, vol. 43, no. 25, pp. 4625–4641, 2023, doi: 10.1523/JNEUROSCI.1091-22.2023.

[8] K. Martínez-Palacios, S. Vásquez-García, O. A. Fariyike, C. Robba, and A. M. Rubiano, "Using Optic Nerve Sheath Diameter for Intracranial Pressure (ICP) Monitoring in Traumatic Brain Injury: A Scoping Review," *Neurocrit. Care*, vol. 40, no. 3, pp. 1193–1212, 2024, doi: 10.1007/s12028-023-01884-1.

[9] N. Jain *et al.*, "Selectivity for food in human ventral visual cortex," *Commun. Biol.*, vol. 6, no. 1, pp. 1–14, 2023, doi: 10.1038/s42003-023-04546-2.

[10] T. Hellas, N. Intelligence, S. Bio-x, H. A. Intelligence, and E. Physics, "Functional connectomics spanning multiple areas of mouse visual cortex," *Nature*, vol. 640, no. 8058, pp. 435–447, 2025, doi: 10.1038/s41586-025-08790-w.

[11] L. Cui, Y. Xiao, Z. Xiang, Z. Chen, C. Yang, and H. Zou, "Study on the correlation between iris blood flow, iris thickness and pupil diameter in the resting state and after pharmacological mydriasis in patients with diabetes mellitus," *BMC Ophthalmol.*, vol. 24, no. 1, pp. 1–9, 2024, doi: 10.1186/s12886-024-03322-y.

[12] S. Ahmed, M. M. Amin, and S. Sayed, "Ocular Drug Delivery: a Comprehensive Review," *AAPS PharmSciTech*, vol. 24, no. 2, pp. 1–29, 2023, doi: 10.1208/s12249-023-02516-9.

[13] A. Kamińska, J. Pinkas, I. Wrześniewska-Wal, J. Ostrowski, and M. Jankowski, "Awareness of Common Eye Diseases and Their Risk Factors—A Nationwide Cross-Sectional Survey among Adults in Poland," *Int. J. Environ. Res. Public Health*, vol. 20, no. 2, pp. 1–20, 2023, doi: 10.3390/ijerph20043594.

[14] A. Scarabosio *et al.*, "Thyroid Eye Disease: Advancements in Orbital and Ocular Pathology Management," *J. Pers. Med.*, vol. 14, no. 7, pp. 1–16, 2024, doi: 10.3390/jpm14070776.

[15] U. Nwagbo and P. S. Bernstein, "Understanding the Roles of Very-Long-Chain Polyunsaturated Fatty Acids (VLC-PUFAs) in Eye Health," *Nutrients*, vol. 15, no. 7, pp. 1–18, 2023, doi: 10.3390/nu15143096.

[16] T. Varzakas and S. Smaoui, "Global Food Security and Sustainability Issues: The Road to 2030 from Nutrition and Sustainable Healthy Diets to Food Systems Change," *Foods*, vol. 13, no. 2, pp. 1–29, 2024, doi: 10.3390/foods13020306.

[17] C. Pinto and D. A. Soares, "Advancements in Glaucoma Diagnosis : The Role of AI in Medical Imaging," *Diagnostics*, vol. 14, no. 4, pp. 1–14, 2024.

[18] G. D. Souza, P. C. S. Mayur, and A. Pandya, "AlterNet K : a small and compact model for the detection of glaucoma," *Biomed. Eng. Lett.*, vol. 14, no. 1, pp. 23–33, 2024, doi: 10.1007/s13534-023-00307-6.

[19] G. N. Patton and H. J. Lee, "Chemical Insights into Topical Agents in Intraocular Pressure Management: From Glaucoma Etiopathology to Therapeutic Approaches," *Pharmaceutics*, vol. 16, no. 2, pp. 1–41, 2024, doi: 10.3390/pharmaceutics16020274.

[20] R. Raveendran *et al.*, "Current Innovations in Intraocular Pressure Monitoring Biosensors for Diagnosis and Treatment of Glaucoma—Novel Strategies and Future Perspectives," *Biosensors*, vol. 13, no. 6, pp. 1–22, 2023, doi: 10.3390/bios13060663.

[21] S. Fujimoto *et al.*, "Macular Retinoschisis from Optic Disc without a Visible Optic Pit or Advanced Glaucomatous Cupping (No Optic Pit Retinoschisis [NOPIR])," *Ophthalmol. Retin.*, vol. 7, no. 9, pp. 811–818, 2023, doi: 10.1016/j.oret.2023.05.020.

[22] J. R. Tribble *et al.*, "Neuroprotection in glaucoma: Mechanisms beyond intraocular pressure lowering," *Mol. Aspects Med.*, vol. 92, no. 6, pp. 1–20, 2023, doi: 10.1016/j.mam.2023.101193.

[23] N. A. Sharif, "Recently Approved Drugs for Lowering and Controlling Intraocular Pressure to Reduce Vision Loss in Ocular Hypertensive and Glaucoma Patients," *Pharmaceuticals*, vol. 16, no. 6, pp. 1–35, 2023, doi: 10.3390/ph16060791.

[24] R. Yamagishi-Kimura, M. Honjo, and M. Aihara, "Effect of a fixed combination of ripasudil and brimonidine on aqueous humor dynamics in mice," *Sci. Rep.*, vol. 14, no. 1, pp. 1–13, 2024, doi: 10.1038/s41598-024-58212-6.

[25] J. M. Micheletti, M. Shultz, I. P. Singh, and T. W. Samuelson, "An Emerging Multi-mechanism and Multi-modal Approach in Interventional Glaucoma Therapy," *Ophthalmol. Ther.*, vol. 14, no. 1, pp. 13–22, 2024, doi: 10.1007/s40123-024-01073-z.

[26] M. F. Cordeiro, S. Gandolfi, K. Gugleta, E. M. Normando, and F. Oddone, "How latanoprost changed glaucoma management," *Acta Ophthalmol.*, vol. 102, no. 2, pp. 140–155, 2024, doi: 10.1111/aos.15725.

[27] E. Konstantakopoulou *et al.*, "Selective Laser Trabeculoplasty After Medical Treatment for Glaucoma or Ocular Hypertension.," *JAMA Ophthalmol.*, vol. 143, no. 4, pp. 295–302, 2025, doi: 10.1001/jamaophthalmol.2024.6492.

[28] T. Hussain and H. Shouno, "Explainable Deep Learning Approach for Multi-Class Brain Magnetic Resonance Imaging Tumor Classification and Localization Using Gradient-Weighted Class Activation Mapping," *Inf.*, vol. 14, no. 11, pp. 1–32, 2023, doi: 10.3390/info14120642.

[29] F. Bagatin, A. Prpic, J. Skunca Herman, O. Zrinscak, R. Ivekovic, and Z. Vatavuk, "Correlation between Structural and Functional Changes in Patients with Raised Intraocular Pressure Due to Graves Orbitopathy," *Diagnostics*, vol. 14, no. 6, pp. 1–13, 2024, doi: 10.3390/diagnostics14060649.

[30] Y. Cheng, M. Yusufu, R. N. Weinreb, and N. Wang, "Dual pressure theory in pathogenesis of glaucomatous optic neuropathy from the Beijing intracranial and intraocular pressure study," *Wiley Interdiscip. Rev. Data Min. Knowl. Discov.*, vol. 1, no. 11, pp. 11–19, 2024, doi: 10.1002/eer3.3.

[31] K. M. Alabdulwahhab, "Diabetic Retinopathy Screening Using Non-Mydriatic Fundus Camera in Primary Health Care Settings – A

Multicenter Study from Saudi Arabia," *Int. J. Gen. Med.*, vol. 16, no. 6, pp. 2255–2262, 2023, doi: 10.2147/IJGM.S410197.

[32] S. D. Browning, J. M. Costello, H. P. Dunn, and C. L. Fraser, "The Use Of Fundus Photography In The Emergency Room A Review," *Curr. Neurol. Neurosci. Rep.*, vol. 25, no. 1, pp. 1–12, 2025, doi: 10.1007/s11910-025-01417-7.

[33] Z. A. T. Ahmed, E. Albalawi, T. H. H. Aldhyani, M. E. Jadhav, P. Janrao, and M. R. M. Obeidat, "Applying Eye Tracking with Deep Learning Techniques for Early-Stage Detection of Autism Spectrum Disorders," *Data*, vol. 8, no. 11, pp. 1–27, 2023, doi: 10.3390/data8110168.

[34] J. I. Lim *et al.*, "Artificial Intelligence Detection of Diabetic Retinopathy," *Ophthalmol. Sci.*, vol. 3, no. 1, pp. 1–8, 2023, doi: 10.1016/j.xops.2022.100228.

[35] M. Ilham, A. Prihantoro, I. K. Perdana, R. Magdalena, and S. Saidah, "Experimenting with the Hyperparameter of Six Models for Glaucoma Classification," *J. Ilm. Tek. Elektro Komput. dan Inform.*, vol. 9, no. 3, pp. 571–584, 2023, doi: 10.26555/jiteki.v9i3.26331.

[36] M. S. Puchaicela-Lozano *et al.*, "Deep Learning for Glaucoma Detection: R-CNN ResNet-50 and Image Segmentation," *J. Adv. Inf. Technol.*, vol. 14, no. 6, pp. 1186–1197, 2023, doi: 10.12720/jait.14.6.1186-1197.

[37] Z. Arif, R. Y. Nur Fu'adah, S. Rizal, and D. Ilhamdi, "Classification of eye diseases in fundus images using Convolutional Neural Network (CNN) method with EfficientNet architecture," *JRTI (Jurnal Ris. Tindakan Indones.*, vol. 8, no. 1, p. 125, 2023, doi: 10.29210/30032835000.

Accredited Rank 2 (Sinta 2) based on the Decree of the Dirjen Penguatan RisBang Kemenristekdikti No.225/E/KPT/2022, December 07, 2022. Published by LPPM Universitas Nusa Mandiri